Charge storage in β-$FeSi_2$ nanoparticles

Jens Theis,[1] Robert Bywalez,[2] Sebastian Küpper,[1] Axel Lorke,[1] and Hartmut Wiggers[2]
[1]*Fakultät für Physik and CENIDE, Universität Duisburg-Essen, D-47048 Duisburg, Germany*
[2]*Institut für Verbrennung und Gasdynamik and CENIDE, Universität Duisburg-Essen, D-47048 Duisburg, Germany*

(Received 25 July 2014; accepted 13 January 2015; published online 2 February 2015)

We report on the observation of a surprisingly high specific capacitance of β-$FeSi_2$ nanoparticle layers. Lateral, interdigitated capacitor structures were fabricated on thermally grown silicon dioxide and covered with β-$FeSi_2$ particles by drop or spin casting. The β-$FeSi_2$-nanoparticles, with crystallite sizes in the range of 10–30 nm, were fabricated by gas phase synthesis in a hot wall reactor. Compared to the bare electrodes, the nanoparticle-coated samples exhibit a 3–4 orders of magnitude increased capacitance. Time-resolved current voltage measurements show that for short times (seconds to minutes), the material is capable of storing up to 1 As/g at voltages of around 1 V. The devices are robust and exhibit long-term stability under ambient conditions. The specific capacitance is highest for a saturated relative humidity, while for a relative humidity below 40% the capacitance is almost indistinguishable from a nanoparticle-free reference sample. The devices work without the need of a fluid phase, the charge storing material is abundant and cost effective, and the sample design is easy to fabricate. © *2015 AIP Publishing LLC*.
[http://dx.doi.org/10.1063/1.4906500]

I. INTRODUCTION

Over the years, β-$FeSi_2$ has repeatedly sparked interest in material science and engineering due to a combination of favorable properties and a potentially wide range of applications. The non-toxic, semiconducting beta phase of $FeSi_2$, which in principle can be manufactured from abundant materials, has been regarded as a capable component for optoelectronic devices, such as photonic crystals in optical telecommunication devices.[1–3] Although featuring an indirect band gap of about 0.78 eV (Refs. 1 and 4), the close lying direct band gap of 0.83–0.89 eV (Refs. 1 and 4) still renders it a valuable choice for photo sensors.[5,6] Moreover, it is a highly interesting material for energy application such as solar cells[5,7–9] since in addition to the favorable band gap, β-$FeSi_2$ exhibits a quite large absorption coefficient of $10^5\,cm^{-1}$. Even thermoelectric generators may profit from this material as it combines a large Seebeck coefficient with relatively high oxidation resistivity.[10–15]

We recently reported on the fabrication of phase pure nanoscale β-$FeSi_2$ by gas phase synthesis,[16] a method enabling easy and large scale production of this material, which may help to boost its marketability. There are only few reports on the synthesis of β-$FeSi_2$ nanoparticles[8,17] and a lack of information regarding their electrical properties. Furthermore, the data obtained on single crystals[4,18,19] and on (doped) polycrystalline thin films[14] may not be directly transferable to nanoparticulate films. Here, we report on detailed investigations of the transport properties of β-$FeSi_2$ nanoparticle films. We find a surprisingly high capability for electrical charge storage, which points towards a yet unexplored potential of this material in energy related technologies.

II. EXPERIMENTAL

A. Nanomaterial properties

The particles were synthesized in a hot wall reactor by decomposition of silane (SiH_4) and ironpentacarbonyle ($Fe(CO)_5$). Details of the reaction kinetics and specific results are given in a previous publication.[16] To confirm the formation of pure β-$FeSi_2$, x-ray diffraction (XRD) measurements were conducted (Fig. 1(a)). The peaks in the diffraction spectrum of our nanoparticles (black curve) correspond to those of β-$FeSi_2$ with a stacking fault probability of 16% (thin red curve).[20] As expected for nanoparticles, the diffraction peaks are broadened in comparison to bulk material.

An analysis with high-resolution transmission electron microscopy (HRTEM) shows that the particles consist of a crystalline β-$FeSi_2$ core, surrounded by an amorphous shell (see inset of Fig. 2(b)), which is rich in silicon and oxygen, but also comprises iron suboxides.[21] To verify the composition of the nanoparticle core and shell, the nanomaterial was analyzed via x-ray photoelectron spectroscopy (XPS). XPS was employed at the Fe2p-signal and the Si2p-signal (Figs. 1(b) and 1(c)). We attribute the peak at 708 eV to $FeSi_2$ and the signal at higher binding energies to the presence of iron suboxides (FeO_x). The Si2p spectrum reveals the presence of SiO_2 and other silicon suboxides (Si_xO_y) in the nanomaterial. XPS measurements in combination with high resolution TEM images lead to the conclusion of an amorphous silicon dioxide shell with a core of iron disilicide. This structure is the result from the different thermal decomposition of SiH_4 and $Fe(CO)_5$ in the reactor. Further examination of the crystallographic structure of these β-$FeSi_2$ nanoparticles was conducted by Imlau *et al.*[22]

The β-$FeSi_2$ crystallites, with sizes in the range of 10–30 nm, form agglomerates in which the single crystallites are often connected by sintering necks.[16] To determine the surface area of the nanoparticles, BET measurements were conducted. The effective surface area for the β-$FeSi_2$ nanoparticles used in this work is about 48.6 m^2/g.

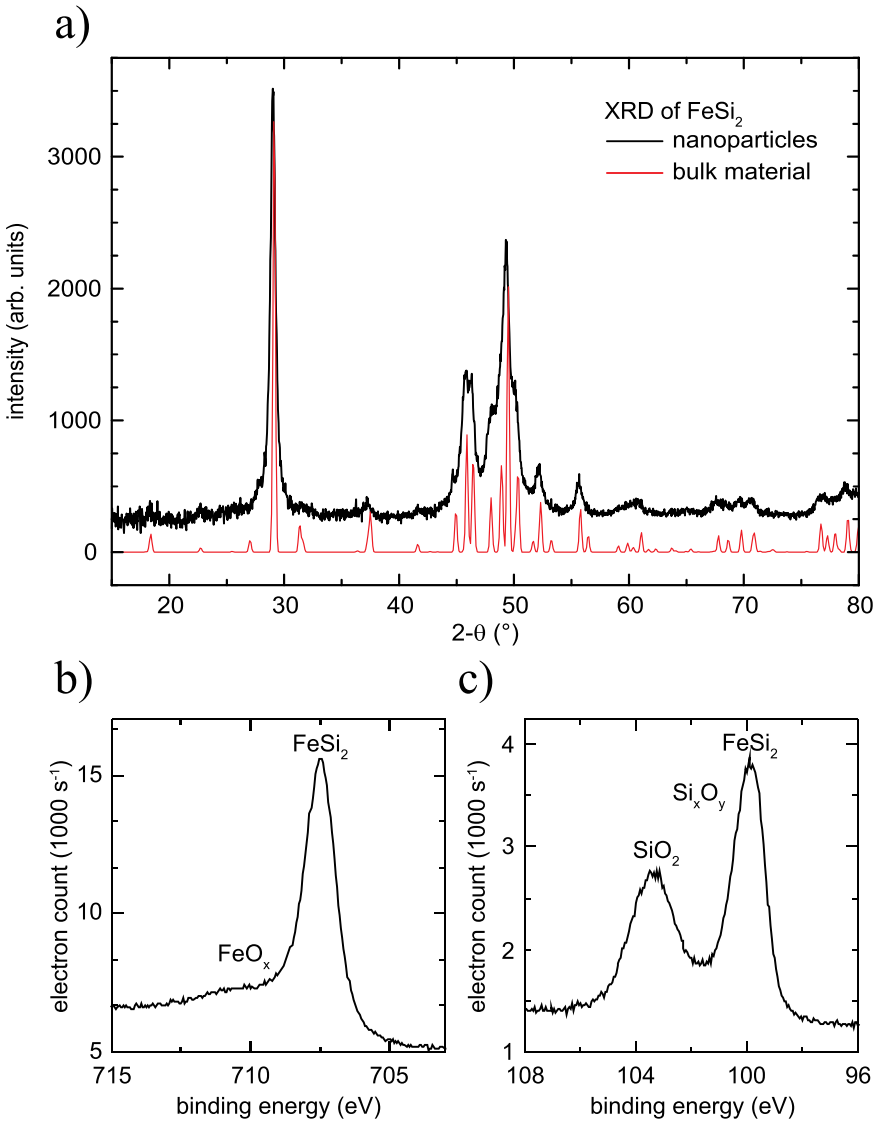

FIG. 1. (a) XRD diagram of the $FeSi_2$ nanoparticles. The XRD peaks of this nanomaterial match those of bulk $FeSi_2$. XPS spectra of the $FeSi_2$ nanoparticles are shown in (b) and (c).

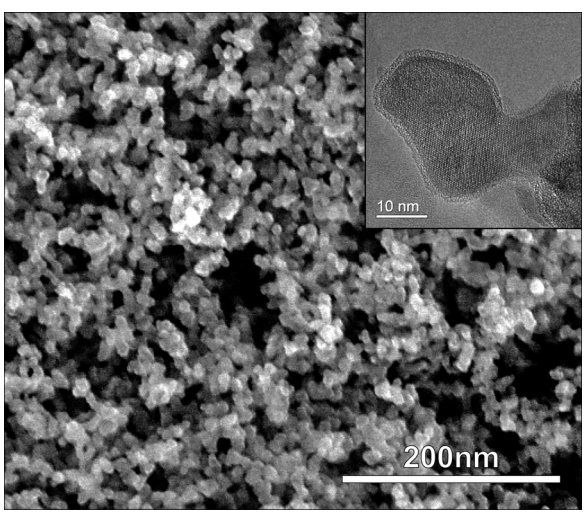

FIG. 2. SEM image of the nanoparticle layer (top view), showing the sponge-like structure of the film. The inset shows a HRTEM picture of a $FeSi_2$ nanoparticle.[16] An amorphous shell around the crystalline core can be observed.

B. Device properties

In order to deposit the particle films, first dispersions of the as-prepared β-$FeSi_2$ nanoparticles were produced. To achieve stable dispersions, 1 to 3 mass percent of β-$FeSi_2$ nanoparticles were dispersed in ethanol (or alternatively water) by ultrasonic treatment. The layers were prepared by a spin casting process at a rotational speed of 250 min^{-1} on gold (or alternatively platinum) interdigitated structures (Fig. 3). The interdigital structures themselves were prepared by optical lithography on p-doped silicon substrates with a 300 nm oxide layer on top. The metal layer consists of 7 nm titanium and 100 nm gold. Each electrode has a width of 20 μm, and the distance between two single fingers of the structure is 48 μm. The effective electrode surface on the substrate is about 1 mm^2. Typical there are 20 μg to 60 μg of β-$FeSi_2$ deposited on the devices, which correspond to a surface area of about 1000 mm^2 to 3000 mm^2. For electrical measurements, the samples were mounted on a chip carrier, and electrical connection was realized by bonding with aluminum wire. All electrical measurements were conducted using a Keithley 2612 source measurement unit.

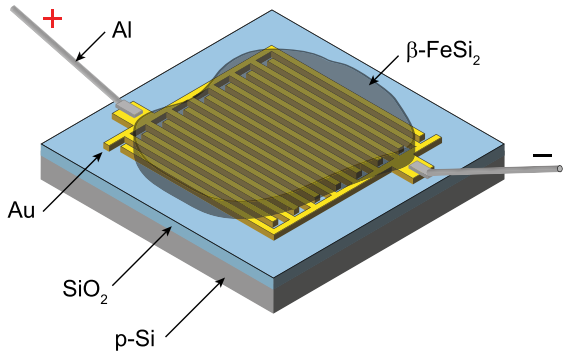

FIG. 3. Schematic design of the sample. Interdigital electrodes are deposited on an oxidized silicon substrate, using standard photo lithography. On top of the structure, the nanoparticle dispersion is spin cast to form a layer of a few micrometers thickness.

Additional SEM and FIB cross-section images of our samples show a porous, homogenous interconnecting network of particles (see also Fig. 2(b)) with film thicknesses of around 6.4 μm. AFM measurements show a film roughness of about 500 nm.

III. RESULTS AND DISCUSSION

In order to study the basic electric properties of the β-$FeSi_2$ nanoparticle films, first the current as a function of the applied voltages was measured, to allow a rough estimation of the film resistance.

Surprisingly, these I-V measurements revealed a pronounced hysteresis as it is the characteristic for highly capacitive materials. Although a magnetic hysteresis has been reported by Hung *et al.* below 100 K for thin films,[23] and at room temperature in β-$FeSi_2$ nanorods, respectively, there are no reports in the literature of an I-V behavior as observed in our samples.

To further investigate the charge storage capability of the nanoparticle layer, the samples were charged at a constant voltage and subsequently discharged. A typical resulting I(t)-curve is shown in Fig. 4(a). Here, for the first two minutes, the sample is charged by applying a constant voltage U_c to the electrodes under the β-$FeSi_2$ nanoparticle film. During charging, an exponential decay of the current is observed until a constant value, the steady state current I_s, is reached. After the charging is complete, the voltage is set to 0 V and the (short circuit) discharging current from the sample is measured for the next five minutes. Here, again, a roughly exponential decay can be observed as the output current approaches zero. The stored charge is determined by integration of the discharge current from of the sample over the discharging time (shaded area in Fig. 4(a)). To exclude any errors deriving from the measurement components, like unknown capacities of cables and chip sockets, we measured an empty reference sample without nanoparticles under the same conditions as the nanoparticle-coated samples (Fig. 4(b)). The results show that this background capacitance is negligible. In addition, measurements at 0 V charging voltage were conducted to identify any offset of the measurement equipment.

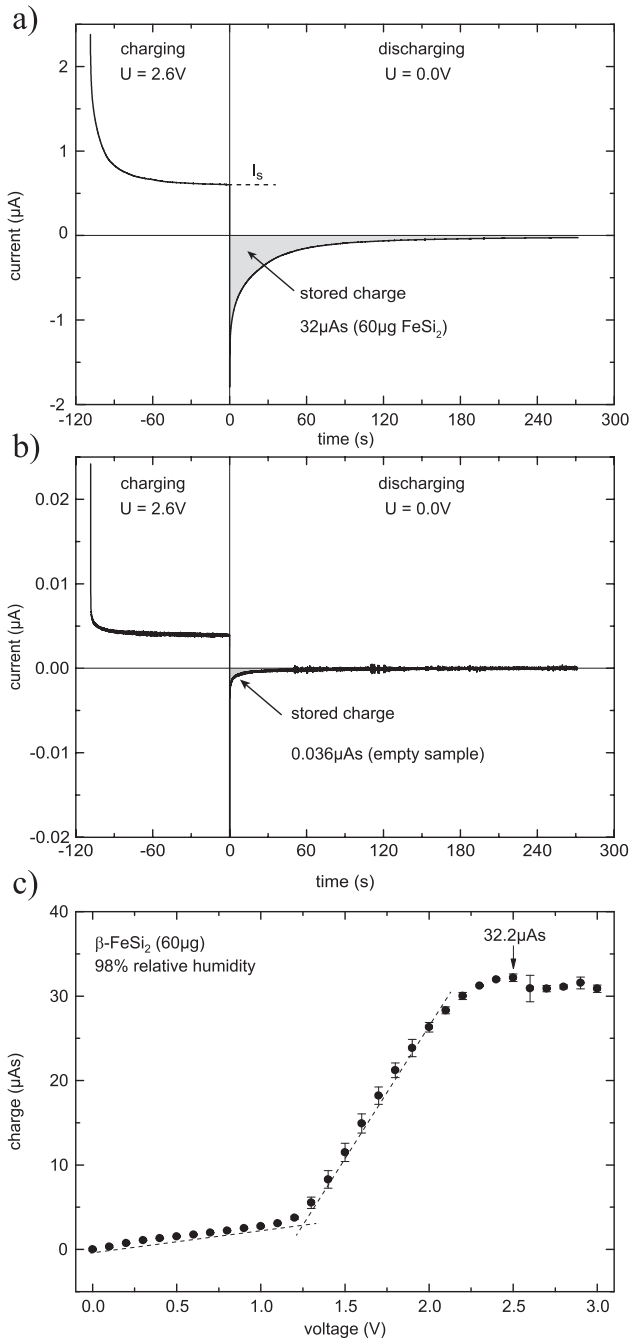

FIG. 4. (a) Typical I(t)-curve of a β-$FeSi_2$ nanoparticle film. After a defined charging time (2 minutes), the stored charge inside the nanoparticle layer is measured by integrating the discharging current (see shaded area). (b) Charging and discharging curve of a nanoparticle-free device with the same parameters as shown in (a). Note the different current scale. (c) Stored charge inside the sample as a function of the charging voltage. Dashed lines are guides to the eye.

A. Transport

For a better understanding of the charge transport inside the β-$FeSi_2$ nanoparticle films, we now turn to the conduction properties of the material. In bulk β-$FeSi_2$, the conduction mechanism is believed to be governed by either small polaron hopping[24] (for a wide range of temperatures) or as variable range hopping (for low temperatures).[25] Our data on β-$FeSi_2$ nanoparticles point towards a slightly different direction. The time dependence of the current shows a

decaying behavior, which asymptotically converges towards a constant value I_S (Fig. 5(a)), which was determined by a biexponential fit. The I(t)-characteristic shows some similarities to measurements of oxidized and etched silicon nanoparticles.[26] It can be modeled using a space charge limited current (SCLC) conduction mechanism, following the relation:

$$I = aV + bV^m. \quad (1)$$

In Fig. 5(b), the steady state current is plotted against the applied voltage. At small voltages, the slope in the double logarithmic plot is around $m_1 = 1.2$, whereas at higher bias the slope is increased to a value of $m_2 = 2.2$. This shows clearly, that for small voltages, the current is governed by an ohmic conduction ($m \approx 1$), whereas at higher bias the effect of the injected charge carriers starts to dominate. In contrast to Pereira *et al.*,[26] who found a transition from ohmic behavior to SCLC in silicon nanoparticles at around 10 V, we find this transition at relatively low voltages of around 1 V.

In the non-ohmic region, the current shows approximately a square power law ($m = 2$), which is the well known Gurney Mott law,[27,28] valid for a material containing defects with a low activation energy. This indicates that even though traps will surely be present in our material, they do not significantly impede the charge transfer further. Also, the exponential decay of the current as observed in our measurements can be explained by the SCLC mechanism. Our data suggest that the trap density is orders of magnitude lower than the free carrier density, thus we suppose that traps are filled initially, building up an electrical field redirecting the current until all traps are saturated and stable conduction paths are available. Probably, a relative large amount of traps is already saturated to start with, so intermediate regions, for example, shallow traps are barely observable.

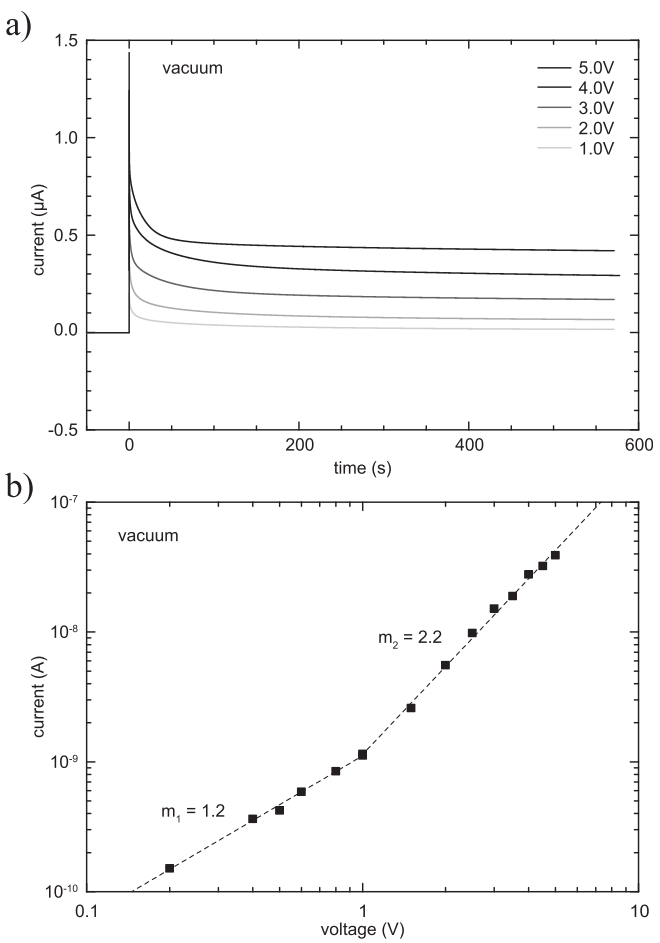

FIG. 5. (a) Time dependent development of the charging current until the steady state current I_S can be observed. The sample is charged at different voltages for a defined time. (b) Double logarithmic plot of the steady state charging current I_S over the charging voltage. Two different conduction regimes are distinguishable by different slopes (dashed lines) m_1 and m_2.

B. Charge storage

To investigate the influence of the charging voltage U_c on the overall stored charge inside the nanoparticle layer, the samples were charged and subsequently discharged at constantly increasing voltages in the range between 0.0 V and 3.0 V. Each measurement is repeated four times to check for reproducibility and improve the signal-to-noise ratio. Afterwards, the stored charge is calculated for every charging voltage U_c and plotted against the charging voltage.

The resulting graph is shown in Fig. 4(c). For low voltages up to 1.2 V, we observe a linear increase in the stored charge inside the nanoparticle layer with increasing voltage U_c, which corresponds to a constant capacitance in this low voltage regime. But at around 1.3 V, a noticeable increase of the discharging current in the I-V curves can be observed. This can be seen in Fig. 4(c) as a sharp bend at 1.3 V. Interestingly, the slope after the bend is again constant for voltages up to 2.0 V. At even higher bias (more than 2 V), the measured charge storage starts to saturate and then even decrease at voltages exceeding 2.5 V. Taking the mass of the nanoparticle film (40 μg) into account, the maximum stored charge corresponds to >0.5 C/g, and values of up to 1 C/g have been observed for other samples. This is a remarkably high value, considering the simplicity of the sample and the setup.

In order to determine that the charge storage is an effect of the entire nanoparticle layer and not due to effects at the substrate-nanoparticle interface or at the electrical contacts, we investigated the influence of the particle layer mass on the stored charge. Samples with three different thicknesses, corresponding to different total β-$FeSi_2$ masses, were prepared by spin casting. One sample was left empty for comparison and to determine the bare capacity of the empty interdigital structure. The results, shown in Fig. 6(a), demonstrate that the stored charge in the nanoparticle layer increases linearly with the deposited β-$FeSi_2$ mass. This is a clear evidence that the charge is stored inside the nanoparticle film. Note that the charge storage of the empty interdigitated structure is almost indistinguishable from zero in Fig. 6(a) and can be neglected with regards to the charge storage.

At present, we cannot give a definite explanation for the mechanism that leads to the remarkable charge storage in the β-$FeSi_2$ films. However, the observation of a bend in Fig. 4(c) at 1.3 V, which separates two regions with different capacitance, is evidence that the charge storage is not only a geometric effect of the sample but also has an electrochemical

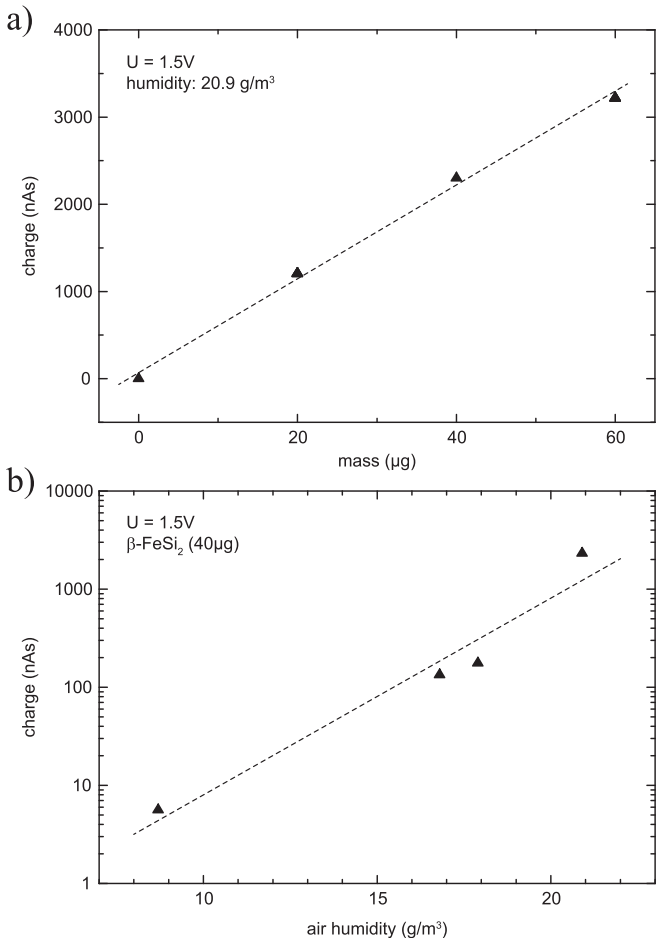

FIG. 6. (a) The stored charge as a function of the mass of the deposited nanoparticle layer. The dashed line is a linear fit to the data. (b) Charge storage capability of the nanoparticle film for different absolute air humidities at room temperature. In the range between 5 and 20 g/m^3, the stored charge increases by 3 orders of magnitude. The dashed line shows an exponential dependence for comparison.

component. Since the first measurements were conducted in ambient air, there were only a few possible reactants to consider. Accordingly, the samples were investigated in vacuum, nitrogen, and dry air. In all these environments, only the geometric capacitance of the samples was relevant and no significant charge storage could be observed. This led us to two conclusions: (1) Even though β-$FeSi_2$ has a high relative permeabillity ϵ_r in the range of $\epsilon_r = 22$ to $\epsilon_r = 170$ (Refs. 25 and 29) and even though the nanoparticle layer increases the surface area between the interdigitated electrodes drastically, both effects are not sufficient to explain the surprisingly large charge storage observed in Fig. 6(b). (2) Water vapor may be a crucial component for the charge storage mechanism.

To measure the exact influence of the air humidity on the stored charge inside the β-$FeSi_2$ nanoparticle layer, the samples were stored and measured in air with controlled humidity. To establish different, well-defined degrees of air humidity, we use the method described in Ref. 30. Four different values of relative humidity, i.e., 30%, 75%, 85%, and 100% (saturation), were investigated, corresponding to 8.7 g/m^3, 16.8 g/m^3, 17.9 g/m^3, and 20.9 g/m^3, respectively. The temperatures during the experiments (21 °C to 26 °C) were measured and a hygrometer was used for monitoring the relative air humidity.

Comparing the stored charge in the nanoparticle layer with the absolute air humidity, there is a clear dependence of the stored charge on the absolute amount of the water content of the air (Fig. 6(b)). Phenomenologically, we find an exponential increase of the stored charge over three orders of magnitude (see dashed line in Fig. 6(b)).

Complementary measurements to confirm the important influence of water vapor to the charge storage process were employed. Cyclic voltammetric (CV) measurements of the β-$FeSi_2$ nanoparticle layer should give a further insight in the process of charge storage inside the device. A triangular voltage sweep was applied and the resulting current was measured. A reference measurement was conducted in vacuum to prohibit any electrochemical reaction with the β-$FeSi_2$ nanoparticle layer (Fig. 7(a)). With no possible reactant present, the I-V curve is a simple oval loop, which is expected for a geometric capacitor. The exposure to dry gases (nitrogen and oxygen) has only negligible influence to the I-V curve. The shape of the I-V curves begins to change as soon as the sample is exposed to humid air (shown in Fig. 7(b)). With increasing humidity, the enclosed surface increases strongly, and at the same time, a changing slope of the curves indicates a reduction in total resistance.

One possible explanation, how water can so profoundly affect the charging of nanoparticle layers, may be the dipole

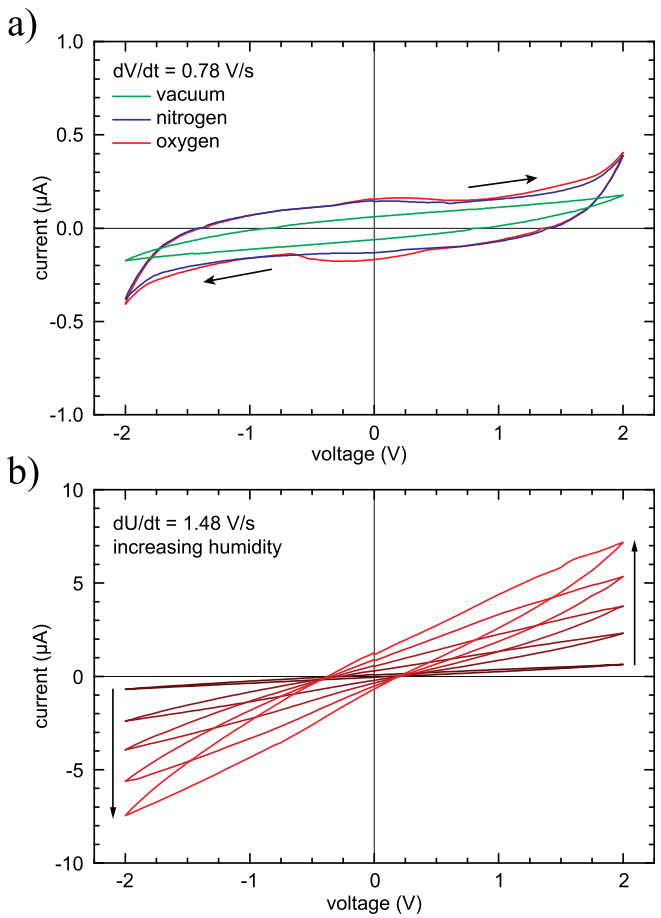

FIG. 7. (a) Cyclic voltammetry measurements of the β-$FeSi_2$ nanoparticle layer under various conditions. No peaks were observed using dry nitrogen or oxygen. (b) CV measurement of the same sample exposed to ambient air. The enclosed area increases with humidity.

moment of H_2O. Adsorbed water on the particle surfaces may very effectively screen the charge inside the particles, similar to the way that water screens the charge of ions in solution by forming a solvation shell. Further investigations are needed to test this assumption. A layer of adsorbed water could also be an explanation for the degrading charge storage capability at voltages higher than 2.5 V (Fig. 4(c)). At such high bias, electrochemical water splitting may occur on the nanoparticles,[31,32] which subsequently would destroy the adsorbed layer of H_2O molecules and thus reduce the charging capability of the device.

In closing, we would like to mention that our findings—even though the exact mechanisms for the charge storage remain to be elucidated—may be of technological interest. The devices are easy to fabricate and the storage medium contains only materials (silicon and iron), that are earth abundant and cost effective. The β-$FeSi_2$ nanoparticles can be synthesized in the gas phase, using processes that are scaleable to industrial quantities.[33] We have found that the devices are robust, show almost no degradation under ambient conditions, and can still be used after months of storage and repeated measurements. While a specific capacity of around 2 F/cm^3 that we find in our samples may not seem impressive compared to today's supercapacitors, it compares favorably to the 1.5 F per cm^3 reported for the first supercapacitor by Becker *et al.*[34] It should be pointed out though that our β-$FeSi_2$ nanoparticle capacitor does not employ any liquid phase or electrolyte, which is a fundamental difference to common supercapacitors. Finally, the pronounced (exponential) sensitivity to the amount of water in the surrounding atmosphere makes our device a promising candidate for gas sensors and detectors.

IV. SUMMARY

We have shown the possibility to store large amounts of electrical charge in a lateral capacitor, consisting of interdigitated electrodes covered by a film of β-$FeSi_2$ nanoparticles. The measured capacity is proportional to the amount of deposited nanoparticles and the specific capacitance of the nanoparticle film is in the range of 1 F per gram. The presence of water molecules in the surrounding atmosphere is essential for the storage capability of the device. Transport measurements show two different conduction regimes. For low voltages, ohmic conduction dominates, whereas for higher voltages transport by SCLC is observed.

ACKNOWLEDGMENTS

This work was supported by CENIDE (Center for Nanointegration Duisburg-Essen) and the Federal Ministry of Education and Research (BMBF) grant 03SF0402A (NADNuM).

[1]V. N. Antonov and O. Jepsen, Phys. Rev. B **57**, 8934 (1998).
[2]Y. Medea, Thin Solid Films **515**, 8118 (2007).
[3]A. Imai, S. Kunimatsu, K. Akiyama, Y. Terai, and Y. Maeda, Thin Solid Films **515**, 8162 (2007).
[4]H. Udono, I. Kikuma, T. Okuno, Y. Masumoto, H. Tajima, and S. Komuro, Thin Solid Films **461**, 182 (2004).
[5]S. Senthilarasu, R. Sathyamoorthy, and S. Lalitha, Sol. Energy Mater. Sol. Cells **82**, 299 (2004).
[6]T. Ootsuka, Z. Liu, M. Osamura, Y. Fukuzawa, N. Otogawa, Y. Nakayama, H. Tanoue, and Y. Makita, Mater. Sci. Eng., B **124–125**, 449 (2005).
[7]M. Powalla and K. Herz, Appl. Surf. Sci. **65/66**, 482 (1993).
[8]N. Dahal and V. Chikan, Chem. Mater. **22**, 2892 (2010).
[9]B. Tatar, K. Kutlu, and M. Uergen, Thin Solid Films **516**, 13 (2007).
[10]Q. S. Meng, W. H. Fan, R. X. Chen, and Z. A. Munir, J. Alloys Compd. **492**, 303 (2010).
[11]L. Han, T. Xin-Feng, C. Wie-Qiang, and Z. Qing-Jie, Chin. Phys. B **18**, 287 (2009).
[12]Y. Qiu, H. L. Shen, Y. G. Yin, and K. H. Wu, Trans. Nonferr. Metal Soc. **17**, 618 (2007).
[13]S. J. Hong, C. K. Rhee, and B. S. Chun, Compd. Solid State Phenom. **118**, 591 (2006).
[14]A. Heinrich, H. Griessmann, G. Behr, K. Ivanenko, J. Schumann, and H. Vinzelberg, Thin Solid Films **381**, 287 (2001).
[15]H. Nagai, S. Katsuyama, S. Nakayama, H. Kobayashi, K. Majima, and M. Ito, Mater. Trans. JIM **39**, 515 (1998).
[16]R. Bywalez, H. Orthner, E. Mehmedovic, R. Imlau, A. Kovacs, M. Luysberg, and H. Wiggers, J. Nanopart. Res. **15**, 1878 (2013).
[17]T. Kameyama, K. Sakanaka, H. Arakawa, A. Motoe, T. Tsunoda, and K. Fukuda, J. Mater. Sci. **28**, 4630–4636 (1993).
[18]K. Gotoha, H. Suzukia, H. Udonoa, I. Kikumaa, F. Esakab, M. Uchikoshic, and M. Isshiki, Thin Solid Films **515**, 8263–8267 (2007).
[19]J. Wang, S. Saitou, S. Ji, Y. Katahira, and M. Isshiki, J. Cryst. Growth **304**, 53 (2007).
[20]H. Yamane and T. Yamada, J. Alloys Compd. **476**, 282 (2009).
[21]R. Bywalez, "Oberflächenmodifikation von silizium- und beta-eisendisilizid nanopartikel für druckbare elektronik" (unpublished).
[22]R. Imlau, A. Kovács, E. Mehmedovic, P. Xu, A. A. Stewart, C. Leidinger, R. E. Dunin-Borkowski, G. Bihlmayer, H. Wiggers, R. Carius, U. Kolb, and M. Luysbergs, Phys. Rev. B. **89**, 054104 (2014).
[23]S.-W. Hung, P.-H. Yeh, L.-W. Chu, C.-D. Chen, L.-J. Chou, Y.-J. Wua, and L.-J. Chen, J. Mater. Chem. **21**, 5704 (2011).
[24]U. Birkholz and J. Schelm, Phys. Status Solidi B **27**, 413–425 (1968).
[25]K. G. Lusunov, E. K. Arushano, C. Kloc, U. Malan, and E. Bucher, Phys. Status Solidi B **195**, 227 (1996).
[26]R. N. Pereira, S. Niesar, W. B. You, A. F. da Cunha, N. Erhard, A. R. Stegner, H. Wiggers, M.-G. Willinger, M. Stutzmann, and M. S. Brandt, J. Phys. Chem. C **115**, 20120 (2011).
[27]N. Mott and R. Gurney, *Electronic Processes in Ionic Crystals*, International Series of Monographs on Physics (Clarendon Press, 1948).
[28]S. Baranovski, *Charge Transport in Disordered Solids With Applications in Electronics*, Wiley Series in Materials for Electronic and Optoelectronic Applications (Wiley, 2006).
[29]P. Hong-Bin, H. Xin, Q. Ru-Dai, C. Lin, and C. Zhi-Ming, Chin. Phys. B **22**, 037301 (2013).
[30]A. Wexler and S. Hasegawa, J. Res. Natl. Bur. Stand. **53**, 19 (1954).
[31]H. J. Yun, H. Lee, J. B. Joo, N. D. Kim, and J. Yi, J. Nanosci. Nanotechnol. **11**, 1688 (2011).
[32]H. N. Nong, L. Gan, E. Willinger, D. Teschner, and P. Strasser, Chem. Sci. **5**, 2955 (2014).
[33]A. Lorke, M. Winterer, R. Schmechel, and C. Schulz, *Nanoparticles from the Gasphase* (Springer, 2012).
[34]H. Becker, "Low voltage electrolytic capacitor," U.S. patent 2,800,616 (1957).